

Mechanism of bending with kinking of a single-walled carbon nanotube

T. Vodenitcharova and L. C. Zhang*

School of Aerospace, Mechanical and Mechatronics Engineering, The University of Sydney, NSW 2006, Australia

(Received 24 October 2003; published 16 March 2004)

This paper explores the mechanism of bending with kinking of a long single-walled carbon nanotube under pure bending with moderate bending angles. The prebuckling response was modeled using the existing continuum mechanics theory accounting for the ovalization of the cross section. The post-buckling behavior was characterized by the development of an elastic kink mechanism, considering the van der Waals force. It was found that the post-buckling strain energy increases almost linearly with the bending angle. The van der Waals force facilitates the kink development and its effect becomes more pronounced at large bending angles.

DOI: 10.1103/PhysRevB.69.115410

PACS number(s): 61.46.+w, 46.70.-p

I. INTRODUCTION

Carbon nanotubes were found to be exceptionally flexible and to undergo reversible deformation to very high strain levels in all generic loading types due to their high bond-breaking resistance.¹⁻⁵ Iijima *et al.*² studied both experimentally and theoretically the deformation properties of carbon nanotubes bent to large angles. They showed that single-walled (SWNT's) and multiwalled nanotubes (MWNT's) could be bent without significant straining up to a critical angle as the outer side of the tube stretched and the inner side compressed. At a critical bending angle, a single V-shaped kink initiated in the inner side subjected to compression, which in the case of MWNT's could be followed by multiple kinks upon further bending. For a SWNT with a radius of 6 Å, molecular dynamics simulations showed a dip in the strain energy vs bending angle curve at an angle of around 27.8° when the nanotube buckled locally and the kink started. Upon further loading the kink advanced with almost a linear energy-bending angle relationship. The top and the bottom walls of the nanotube were found to be separated by a gap of around 3.5 Å, at which the van der Waals interaction became strongly repulsive. Upon complete unloading from angles below 110° the nanotube completely recovered. However, at a very large bending angle of 120° atomic bonds broke and the nanotube's deformation became irreversible.

Further studies confirmed the above observations. Yakobson *et al.*¹ conducted similar MD simulations on the bending of nanotubes but additionally studied the response of the tubes to axial loading and torsion. They noticed the similarities in the behavior of carbon nanotubes and macroscopic shells and suggested that the continuum theories of shell structures can be of use in predicting the behavior of carbon nanotubes.

The bending of macrotubes has been well investigated.⁶⁻¹⁸ Mamalis *et al.*¹³ experimentally observed three collapse modes of circular tubes in plastic bending, i.e., a V-shaped kink with triangular regions in the compressive wall, a similar kink but additionally supplemented by bulges parallel to the hinge line and a fractural failure in the tensile side of the kink due to excessive stretching. In the first collapse mode, they found that at a small bending angle of around 10° the tube started folding, i.e., a kink was initiated, and the bending moment started to decrease steadily from its

peak at the point of local buckling. The kink was associated with the development of plastic deformation. However, the application of continuum mechanics to a carbon nanotube, a discrete structure, requires knowledge of geometrical parameters (e.g., equivalent thickness t), material properties (e.g., equivalent Young's modulus E), and effect of van der Waals forces. The present paper aims to develop a predictive mechanics model to describe the bending-kinking response of nanotubes under pure bending, using the equivalent nanotube thickness ($t=0.617$ Å) and the equivalent Young's modulus (4.88 TPa) clarified recently.¹⁹

II. MODELING

Consider the elastic bending of a single-walled nanotube subjected to an external bending moment M [Fig. 1(a)]. With increasing the load the tube bends and flattens, as both experiments and MD simulations showed. Since the dominant internal stress in pure bending is in the longitudinal direction, the circumferential direct strain is negligible and the formulas for inextensional bending with flattening can be applied. Additionally, it is reasonable to accept that the strain is small before local buckling (or kinking) is initiated at a small bending angle. Bending of circular tubes with the above deformation characteristics was studied by Brazier, as summarized in many references.^{6,17,18} For convenience, relevant formulas are listed in the Appendix.

Before kinking, the flattening of a nanotube's cross section during bending can be described by the flattening ratio ζ

$$\zeta = \frac{R - R_c}{R}, \quad (1)$$

where R is the initial radius of the tube and R_c is the current radius (along the small semi-axis) varying with the bending angle ψ . The normal and tangential displacements are, respectively [Fig. 1(a)]

$$w = R\zeta \cos 2\theta, \\ v = -\frac{1}{2} R\zeta \sin 2\theta. \quad (2)$$

With the increase of the external bending moment, the axial compression in the tube increases as well, and when the compressive stress reaches a critical value, the tube will lo-

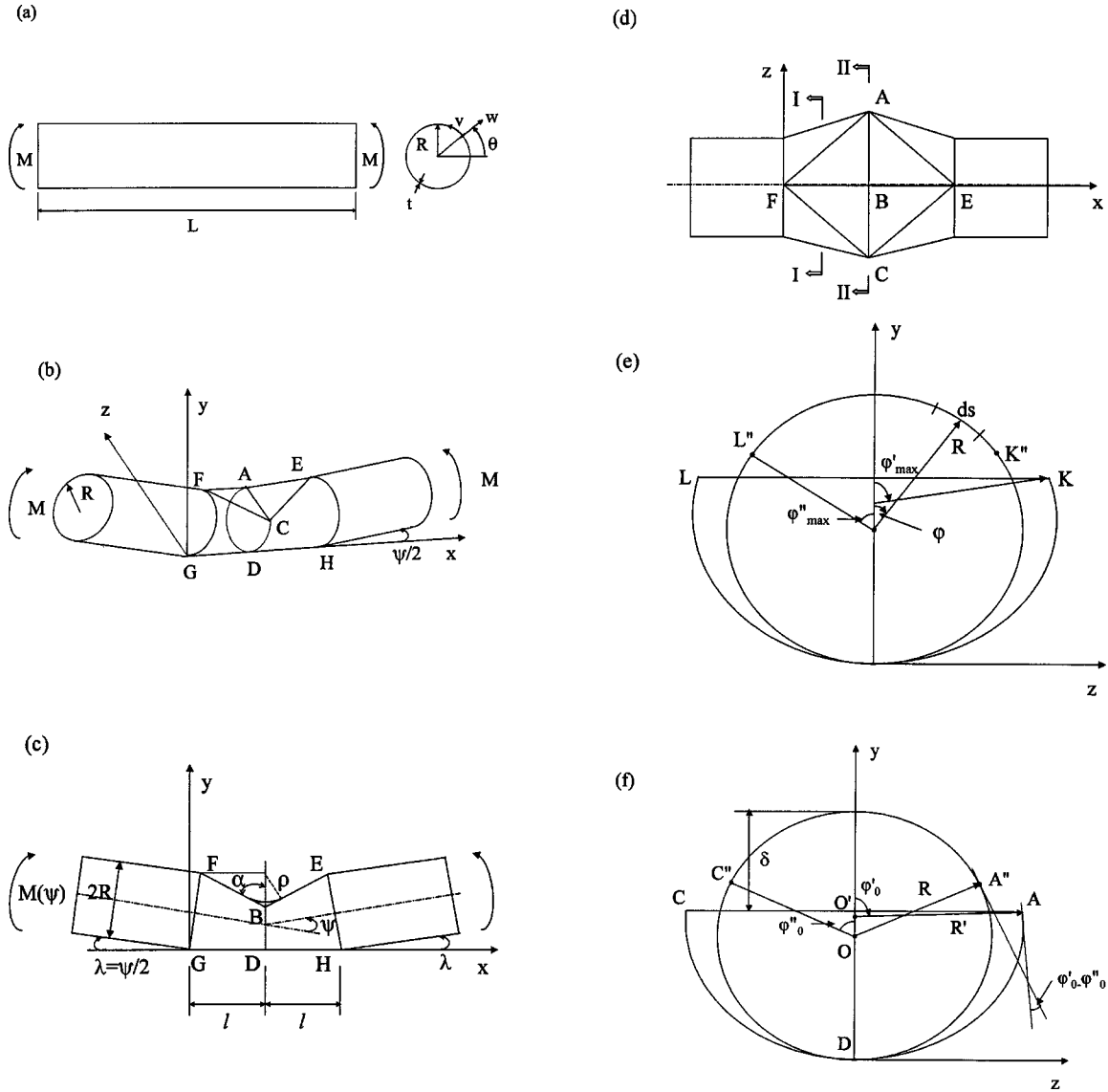


FIG. 1. (a) Nanotube geometry, where L is the length, R is the mean radius, t is the wall thickness, θ is the circumferential coordinate, and M is the external bending moment. (b) Kink mechanism of a nanotube under bending. (c) Side view of (b). (d) Top view of (b). (e) Cross section $I-I$ of (d). (f) Cross section $II-II$ of (d).

cally buckle. The value of ζ at the point of local buckling is around 0.14 (see the Appendix).

Once the kink has started, the nanotube becomes a mechanical mechanism and the formulas in the Appendix are no longer valid. Relevant experiments and molecular dynamics simulations suggest that the pattern of the deformation resembles the kink mechanism similar to that of a macrotube.¹³ A portion of the wall flattens and forms two triangular plates ACF and ACE [Figs. 1(b)–1(d)] that rotate about a central hinge line AC . The remaining part of the tube remains circular although it flattens and decreases its curvature. The borders between the triangular zones and the circular zones are hinge lines AE , CE , AF , and CF . The collapse mode of folding is nearly inextensional and the hinges could be viewed as stationary. Since a carbon nanotube elastically deforms even after kinking, the hinges in the above kink mechanism are elastic.

The formulation is based on two continuity conditions, in the circumferential direction of the tube and in the tube's longitudinal direction. The cross-section deforms in such a way that a circular arc $A''C''$ defined by a central angle ϕ''_0 , flattens and produces a hinge line AC [Fig. 1(e)–1(f)]. This condition differs from the condition $AC = 2\phi_0 R$ (Ref. 13) in macrotubes of small collapsing angles and avoids the cross section jamming at angles very close to the angles of kinking initiation. The length of AC is calculated as

$$AC = A''C'' = 2R\phi''_0. \tag{3}$$

On the other hand, it is obvious that

$$AC = 2AB = 2R' \sin \phi'_0, \tag{4}$$

where R' is the radius of the bottom arc ADC as shown in Fig. 1(f).

Equations (3), (4) lead to

$$R\varphi_0'' = R' \sin \varphi_0', \quad (5)$$

therefore,

$$\varphi_0'' = \frac{R' \sin \varphi_0'}{R}. \quad (6)$$

Further, the length of the bottom arc AGC is calculated by

$$AGC = 2R'(\pi - \varphi_0'). \quad (7)$$

For an inextensional cross section, the perimeter remains unchanged, i.e., $AC + AGC = 2\pi R$, hence

$$2R\varphi_0'' + 2R'(\pi - \varphi_0') = 2\pi R \quad (8a)$$

or

$$2R \sin \varphi_0' + 2R'(\pi - \varphi_0') = 2\pi R. \quad (8b)$$

Additionally, parameters R' and φ_0' are linked to the deformation in the longitudinal direction through parameter δ defined in Ref. 12:

$$R' + R' \cos \varphi_0' = 2R - \delta. \quad (9)$$

From Eq. (8a) one gets

$$R' = \frac{\pi R}{\sin \varphi_0' + \pi - \varphi_0'}. \quad (10)$$

The coordinates of point A , expressed in terms of the bending angle ψ , are $x_A = l$, $y_A = 2R \cos(\lambda) - [2R \sin \lambda(2l - 2R \sin \lambda)]^{1/2}$ and $z_A = R' \sin \varphi_0'$. The length of the kink $2l$ is assumed to be equal to $2R$ (Ref. 13) and the drop in the cross section δ is

$$\delta = 2R - y_B. \quad (11)$$

Further,

$$\alpha = a \sin \left(1 - \frac{2R}{l} \sin \lambda \right), \quad (12)$$

and the length of each of the hinge lines AE , CE , AF , CF is

$$l_h = \sqrt{l^2 + AB^2}. \quad (13)$$

Here the tube mechanism deforms elastically. Hence, the bending moments are calculated using the plate/shell theory considering the curvatures in bending. The top cylindrical part of the kink in its unstrained position has a curvature in the circumferential direction of $(1/R)$. After local buckling, it flattens into the triangular zones ACF and ACE , undergoing a curvature change of $(-1/R)$. Therefore, the bending moment in the circumferential direction θ is

$$M_{\theta\theta} = \frac{1}{R} \frac{Et^3}{12(1-\mu^2)}, \quad (14)$$

where μ is the Poisson's ratio and the corresponding work done in flattening, or stored energy, is

$$W_1 = 4M_{\theta\theta}R\varphi_0''. \quad (15)$$

The bottom circular region, initially with a circumferential curvature of $(1/R)$, flattens to an arc with a curvature of $(1/R')$ during kinking. Then, the bending moment M_2 in the circumferential direction is given by

$$M_2 = - \left(\frac{1}{R'} - \frac{1}{R} \right) \frac{Et^3}{12(1-\mu^2)} \quad (16)$$

and the stored strain energy becomes

$$W_2 = 4M_2R(\pi - \varphi_0'')(\varphi_0' - \varphi_0''). \quad (17)$$

Both the triangular parts of the kink rotate about a stationary hinge line AC with a relative angle of rotation $(\pi - 2\alpha)$. The elastic bending moment M_{xx} working during this rotation is in the x direction. In order to calculate this quantity, one needs to evaluate the curvature change $(1/\rho)$ of the plates locally at the location of the hinge [Fig. 1(c)] although the plates in the kink mechanism are considered flat. It is evident that for $\alpha = \pi/2$ (undeformed tube) the local curvature $(1/\rho)$ is 0. With the development of the kink, the local curvature increases, as the two parts of the kink cannot get closer than the equilibrium distance of $d_{eq} = 3.42 \text{ \AA}$. For $\alpha = 0$ (full flattening), the distance between the opposite walls is exactly equal to the equilibrium distance and an arc is formed with a curvature $(1/\rho) = (3.42/2) \text{ \AA}$. As a first approximation, the variation of the local curvature with α can be considered linear in the range of $\pi/2$ to 0. This leads to

$$M_{xx} = \left(\frac{2}{d_{eq}} \frac{\pi - 2\alpha}{\pi} \right) \frac{Et^3}{12(1-\mu^2)}. \quad (18)$$

The strain energy then becomes

$$W_3 = M_{xx}(\pi - 2\alpha)AC. \quad (19)$$

At hinge lines AE , CE , AF , and CF the elastic moment in the direction perpendicular to the hinges is obtained by resolving the moments $M_{\theta\theta}$ and M_{xx} (being zero in the flattened triangular parts)

$$M_{nn} = M_{xx} \cos^2 \varepsilon_x + M_{\theta\theta} \sin^2 \varepsilon_x, \quad (20)$$

where ε_x is the angle between the normal to the hinge line and the longitudinal x direction, i.e.,

$$\varepsilon_x = a \tan \left(\frac{l}{AB} \right). \quad (21)$$

Then the strain energy at each of the four hinge lines is

$$W_4 = \frac{2M_{nn}l_h^2\varphi_0'}{l}. \quad (22)$$

Thus, as the bending angle ψ varies, the elastic moments in the plates of the kink mechanism vary as well and as a consequence the total work done by the external load, being the sum of all four strain energies, is a function of the bending angle $W(\psi)$, i.e.,

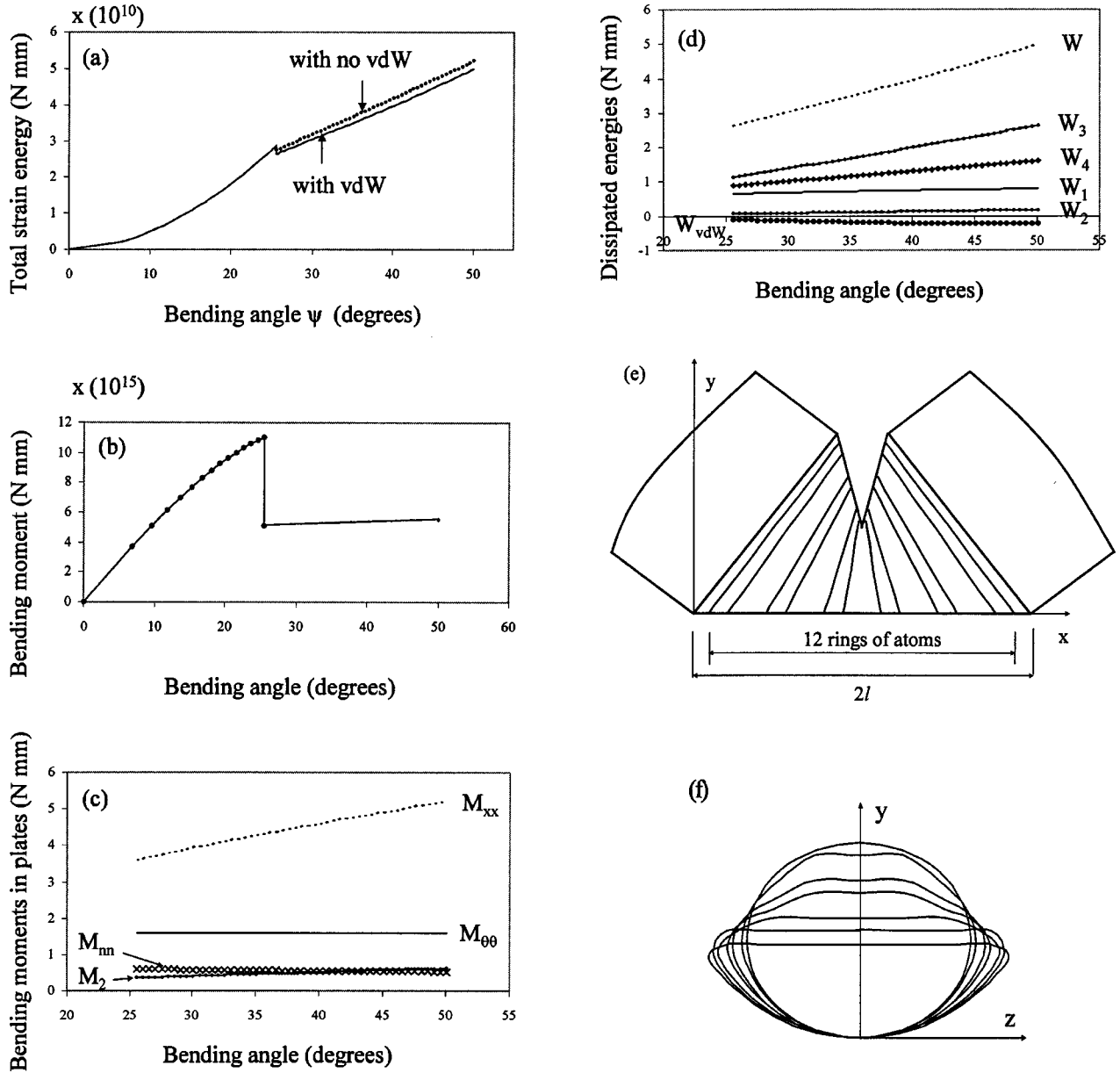


FIG. 2. (a) Total strain energy of a nanotube with $R=6.26 \text{ \AA}$. (b) Bending moments M vs bending angle. (c) Elastic bending moments in the plates of the kink varying with the bending angle. (d) Work done in the kink mechanism, where W_1 is the work done in flattening of the triangular regions, W_2 is the work done in flattening of the circular region, W_3 is the work done in rotation about hinge line AC , W_4 is the work done in rotation about hinge lines AE , CE , AF and CE , W_{vdW} is the work done by the van der Waals force and W is the total work done. (e) Longitudinal section through the kink at bending angle of 52.4° (not to scale). (f) Cross-sectional view of the deformed atomic rings at bending angle of 52.4° .

$$W(\psi) = \sum_{i=1}^4 W_i. \tag{23}$$

With the known W , the external bending moment at any bending angle is calculated as the derivative $dW/d\psi$. Equation (23) evaluates the elastic work absorbed in the tube during the bending process due to mechanical loads only. However, the bending of a nanotube differs from that of a macrotube because in the former van der Waals forces play an important role when kinking appears.

III. WORK DONE BY THE VAN DER WAALS FORCE

The van der Waals force accounts for the interaction between the opposite walls of the nanotube when they approach each other. The magnitude of the force depends on the distance between the atoms. For large distances, the van der Waals force is attractive, but when the separation between the atoms is below the equilibrium distance of 3.42 \AA , it becomes strongly repulsive. In the case of pure bending of nanotubes the van der Waals interaction appears when the kink starts. With the increase in the bending angle, the top and bottom parts of the kink get closer to each other, and at

a certain stage, the distance between them reaches the equilibrium distance. Upon additional bending, this distance remains unchanged because there are no external normal loads applied on the walls to prevail over the repulsive van der Waals forces.

The van der Waals force between atom i and j can be expressed by the Lennard-Jones potential as

$$U_{ij}(r_{ij}) = 4\varepsilon \left(\frac{\sigma^{12}}{r_{ij}^{12}} - \frac{\sigma^6}{r_{ij}^6} \right), \quad (24)$$

where $\varepsilon = 4.7483 \times 10^{-19}$ (N mm), $\sigma = 3.407$ Å, and r_{ij} is the distance between the two atoms. Then, the total potential for the nanotube U_{vdW} , is the sum of the contribution of all atoms. The work done by the van der Waals force for each atom is the product of the force and the displacement of the atom during the deformation of the kink. Bearing in mind that the van der Waals force is potential, the total work done by this force during the bending of the tube W_{vdW} can be calculated as the increase in the total tube potential from the initial unstrained state to the current strained state corresponding to the current bending angle ψ , incorporating the location details of the atoms in the kink according to the chirality of the nanotube and the geometry of the kinking mechanism developed in the previous section.

IV. RESULTS AND DISCUSSION

As an example, a nanotube with a radius of 6.26 Å is considered. The elastic modulus and the thickness are $E = 4.88$ TPa and $t = 0.617$ Å, respectively, according to our previous clarification.¹⁹ The Poisson's ratio adopted is 0.19.¹ The Brazier theory (see the Appendix) holds up to the point of local buckling at $\psi = 25.58^\circ$. Below this point, the elastic energy calculated by Eqs. (A4)–(A5) is nonlinear [Fig. 2(a)] but the bending moment $M(\psi)$ increases quite linearly up to about $\psi = 20^\circ$ [Fig. 2(b)].

When kink happens, the absorbed energy during bending is almost linear and the corresponding bending angle is almost constant. The elastic bending moments in the upper triangular plates, bottom arc, along hinge lines AC , AE , CE , AF , and CF are plotted in Fig. 2(c). It is clear that the moment in hinge AC , M_{xx} , is dominant because in the kink the local curvature at that location is large, as confirmed by the results shown in Fig. 2(d), where W_3 is the work done by M_{xx} .

In order to calculate the work done by the van der Waals force W_{vdW} one needs to know the initial and current (at varying bending angle ψ) positions of the carbon atoms. Before deformation, circumferentially the atoms are at a distance of $S = 1.42\sqrt{3}$ Å but longitudinally they are clustered into rings at an alternating distance of 0.71 or 1.42 Å. During bending the atoms move following the deformation of the kink, as quantitatively evaluated in Sec. II. It is reasonable to assume that the tube cross sections remain planar during kinking and the increments in the coordinates of the atoms vary linearly between the corresponding atoms in the end cross sections. The length of the kink $2l$ accommodates twelve rings; at $\psi = 52.4^\circ$ the longitudinal view of the rings

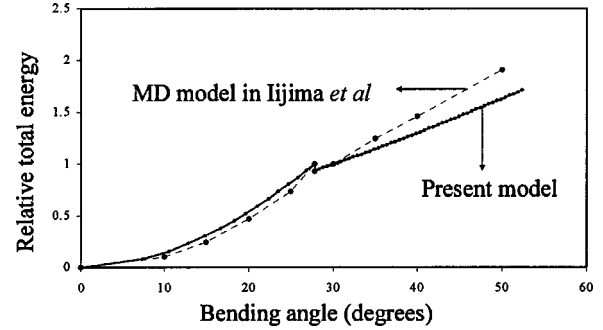


FIG. 3. Comparison between the relative energies in the present model and in Ref. 2 ($R = 6$ Å).

is shown in Fig. 2(e) and the cross-sectional view is plotted in Fig. 2(f).

The initial deformation of the cross sections $x = 0$ and $x = 2l$ at local buckling is taken into account; however, its influence is negligible. The values of the work done by the van der Waals force are negative, as shown in Fig. 2(d). This is expected as the van der Waals force is rather an “external” load than a resistance force and its work is added to the work done by the external moment $M(\psi)$. In the calculation of the van der Waals force, we consider only the interaction between the top and bottom walls of the kink and introduce a cutoff of 3 Å. The interaction between the two sides of the top surface, which are inclined at an angle of 2α , is neglected. This assumption is close to the real behavior of kinking. As the kink develops, the equilibrium distance of 3.42 Å is quickly reached. Further increase of the bending angle ψ does not decrease the distance between the sidewalls because there is no lateral load to force the walls getting closer and overcome the large repulsive force.

Iijima *et al.*² reported that the kinking of a nanotube of radius $R = 6$ Å occurs at an angle of about 27.8° . Further development of the kink is associated with an almost linear increase of the strain energy. The present model, when applied to the same nanotube, showed almost exactly the same critical bending angle of 27.9° . Comparing the strain energies (Fig. 3) the present model produces before kinking slightly higher relative strain energy (i.e., the ratio of the strain energy at ψ and the strain energy at the critical buckling angle just before kinking). At the point of kinking, the model gives the same drop in energy as the molecular dynamics simulation predicted. Upon further increase of the bending angle, however, the present model yields lower values of strain energy and lower bending moments. Therefore, more accurate kinking mechanism, especially the longitudinal curvature development in the compressed part of the kink, needs to be established.

V. CONCLUSIONS

This paper has established a mechanics model for the bending mechanism of a SWNT with kinking. The prebuckling deformation involves the ovalization of the tube cross section and the post-buckling deformation takes into account flattening and the van der Waals force. A new concept of elastic hinges is introduced to reflect the large elastic defor-

mation. The prediction of the model, including the variation of strain energy and the stiffening of the nanotube is consistent with the existing experimental observations and molecular dynamics simulations. This model and its associated deformation mechanism describe clearly the bending-kinking process of a SWNT and offer a convenient tool for the mechanical characterization of SWNT's of various diameters.

ACKNOWLEDGMENT

This work was supported by an ARC Discovery Grant.

APPENDIX: BRAZIER THEORY

Consider a tube of thickness t , radius R , length L , Young's modulus E , and Poisson's ratio μ . The curvature of the tube axis in the longitudinal direction C is expressed as

$$C = \frac{2ct}{R^2(1-\mu^2)\sqrt{3}}, \quad (\text{A1})$$

where c is the nondimensional curvature defined as

$$c = \frac{\sqrt{3}\zeta}{2}. \quad (\text{A2})$$

The strain energy per unit length U is given by

$$U = \frac{1}{2}C^2E\pi R^3t \left(1 - \frac{3}{2}\zeta + \frac{5}{8}\zeta^2\right) + \frac{3\pi Eth^2\zeta^2}{8R}, \quad (\text{A3})$$

where the first term is the contribution of the longitudinal stretching of the ovalized cross section and the second term is the contribution of the circumferential bending during ovalization as a ring.

Then, the total tube energy is

$$U_t = UL \quad (\text{A4})$$

and the bending moment is

$$M = \frac{dU_t}{d\psi}. \quad (\text{A5})$$

For axial compression, the critical compressive stress is

$$\sigma_{cr} = \frac{N}{t} = -\frac{EtR}{\sqrt{3(1-\mu^2)}}, \quad (\text{A6})$$

where N is the axial load.

The elementary bending theory, which gives no consideration to the flattening effect, leads to a critical bending moment in local buckling M_{cr}

$$M_{cr} = \frac{\pi ERth}{\sqrt{3}},$$

$$h = \frac{t}{\sqrt{1-\mu^2}}. \quad (\text{A7})$$

However, the flattening will decrease the value of the critical bending moment M

$$M = mM_{cr}, \quad (\text{A8})$$

where m is derived as

$$m = 2c(1-2c^2). \quad (\text{A9})$$

For small values of ζ the radius of the local curvature at the point of the maximum compressive stress is calculated as

$$\rho = \frac{R}{1-3\zeta}. \quad (\text{A10})$$

Thus, the maximum compressive stress will be a fraction of the critical compressive stress predicted by the elementary beam theory

$$\sigma = s\sigma_{cr}, \quad (\text{A11})$$

where s is called dimensionless extreme fiber stress.

It is assumed that the compressive stress at local buckling depends on the local curvature so that

$$s_{cr} = \frac{R}{\rho}. \quad (\text{A12})$$

The compressive strain is therefore

$$\varepsilon = CR(1-\zeta). \quad (\text{A13})$$

From Fig. 16.7(a) of Ref. 6 the point of intersection of s_{cr} and s corresponds to the point of local buckling with $\zeta = 0.14$. For ζ up to 0.14, the quantities above are calculated as functions of ζ , resulting in the graph in Figs. 2(a), 2(b) for the prebuckling behavior of the nanotube.

*E-mail address: zhang@aeromech.usyd.edu.au

¹B. I. Yakobson, C. J. Brabec, and J. Bernholc, Phys. Rev. Lett. **76**, 2511 (1996).

²S. Iijima, C. Brabec, A. Maiti, and J. Bernholc, J. Chem. Phys. **104**, 2089 (1996).

³D. Srivastava, D. W. Brenner, S. J. David, K. D. Ausman, M.-F. Yu, and R. S. Ruoff, J. Phys. Chem. B **103**, 4330 (1999).

⁴M.-F. Yu, M. J. Dyer, and R. S. Ruoff, J. Appl. Phys. **89**, 4554 (2001).

⁵G. Gao, T. Cagin, and W. A. Goddard III (unpublished).

⁶C. R. Calladine, *Theory of Shell Structures* (Cambridge University Press, Cambridge, 1983).

⁷E. Corona and S. Kyriakides, Int. J. Solids Struct. **24**, 505 (1988).

⁸G. H. Daneshi and S. J. Hosseini-pour, J. Mater. Process. Technol. **125–126**, 826 (2002).

⁹P. Drazetic, F. Payen, E. Ducrocq, and E. Markiewicz, Thin-Walled Struct. **33**, 155–176 (1999).

¹⁰S. Gellin, Int. J. Solids Struct. **16**, 397 (1980).

¹¹S. A. Karamanos, Int. J. Solids Struct. **39**, 2059 (2002).

¹²D. Kecman, Int. J. Mech. Sci. **25**, 623 (1983).

¹³A. G. Mamalis, D. E. Manolacos, K. Baldoukas, and G. L. Viegelahn, Proc. Inst. Mech. Eng. **203**, 411–417 (1989).

- ¹⁴E. Markiewicz, F. Payen, D. Cornette, and P. Drazetic, *Thin-Walled Struct.* **33**, 177 (1999).
- ¹⁵N. K. Prinja and N. R. Chitkara, *Nucl. Eng. Des.* **83**, 113 (1984).
- ¹⁶K. C. Shin, J. J. Lee, K. H. Kim, M. C. Song, and J. S. Huh, *Compos. Struct.* **57**, 279 (2002).
- ¹⁷T. X. Yu and L. C. Zhang, *Plastic Bending: Theory and Applications* (World Scientific, Singapore, 1996).
- ¹⁸L. C. Zhang and T. X. Yu, *Int. J. Pressure Vessels Piping* **30**, 77 (1987).
- ¹⁹T. Vodenitcharova and L. C. Zhang, *Phys. Rev. B* **68**, 165401 (2003).